6. Higuchi, H., Nakauchi, Y., Maruyama, K. & Fujime, S. Characterization of α-connectin from striated muscle by dynamic light scattering. *Biophys. J.* **65,** 1906–1915 (1993).
7. Wang, K., McCarter, R., Wright, J., Beverly, J. & Ramirez-Mitchell, R. Viscoelasticity of the sarcomere matrix of skeletal-muscles: the titin-myosin composite filament is a dual-stage molecular spring. *Biophys. J.* **64,** 1161–1177 (1993).
8. Soteriou, A., Clarke, A., Martin, S. & Trinick, J. Titin folding energy and elasticity. *Proc. R. Soc. Lond. B* **254,** 83–86 (1993).
9. Erickson, H. P. Reversible unfolding of fibronectin type-III and immunoglobulin domains provides the structural basis for stretch and elasticity of titin and fibronectin. *Proc. Natl Acad. Sci. USA* **91,** 10114–10118 (1994).
10. Politou, A. S., Thomas, D. J. & Pastore, A. The folding and stability of titin immunoglobulin-like modules, with implications for the mechanism of elasticity. *Biophys. J.* **69,** 2601–2610 (1995).
11. Flory, P. J. in *Statistical Mechanics of Chain Molecules* 316–304 (Hanser, Munich, 1989).
12. Fixman, M. & Kovac, J. Polymer conformational statistics. III. Modified Gaussian models of stiff chains. *J. Chem. Phys.* **56,** 1564–1568 (1973).
13. Kellermayer, M. S. Z. & Granzier, H. L. Elastic properties of single titin molecules made visible through fluorescent F-actin binding. *Biochem. Biophys. Res. Comm.* **221,** 491–497 (1996).
14. Linke, W. A., Bartoo, M. I., Ivemeyer, M. & Pollack, G. H. Limits of titin extension in single cardiac myofibrils. *J. Muscle Res. Cell Motil.* **17,** 425–438 (1996).
15. Politou, A. S., Gautel, M., Pfuhl, M., Labeit, S. & Pastore, A. Immunoglobulin-type domains of titin: same fold, different stability? *Biochemistry* **33,** 4730–4737 (1994).
16. Fong, S. *et al.* Structure and stability of an immunoglobulin superfamily domain from twitchin, a muscle protein of the nematode *Caenorhabditis elegans. J. Mol. Biol.* **264,** 624–639 (1996).
17. Litvinovich, S. V., Novokhatny, V. V., Brew, S. A. & Ingram, K. C. Reversible unfolding of an isolated heparin and DNA binding fragment, the first type III module from fibronectin. *Biochim. Biophys. Acta* **1119,** 57–62 (1992).
18. Plaxco, K. W., Spitzfaden, C., Campbell, I. D. & Dobson, C. M. Rapid refolding of a proline-rich all-beta-sheet fibronectin type-III module. *Proc. Natl Acad. Sci. USA* **93,** 10703–10706 (1996).
19. Soteriou, A., Gamage, M. & Trinick, J. A survey of the interactions made by the giant protein titin. *J. Cell Sci.* **104,** 119–123 (1993).
20. Whiting, J., Wardale, J. & Trinick, J. Does titin regulate the length of muscle thick filaments. *J. Mol. Biol.* **205,** 263–268 (1989).
21. Fürst, D. O., Osborn, M., Nave, R. & Weber, K. The organisation of titin filaments in the half-sarcomere revealed by monoclonal-antibodies in immunoelectron microscopy: a map of ten nonrepetitive epitopes starting at the Z-line extends close to the M-line. *J. Cell Biol.* **106,** 1563–1572 (1988).
22. Simmons, R. M., Finer, J. T., Chu, S. & Spudich, J. A. Quantitative measurements of force and displacement using an optical trap. *Biophys. J.* **70,** 1813–1822 (1996).
23. Bustamante, C. Entropic elasticity of λ-phage DNA. *Science* **265,** 1599–1600 (1994).
24. Tskhovrebova, L. & Trinick, J. Direct visualization of extensibility in isolated titin molecules. *J. Mol. Biol.* **265,** 100–106 (1997).
25. Rief, M., Gautel, M., Oesterhelt, F., Fernandez, J. M. & Gaub, H. E. Reversible unfolding of individual titin Ig-domains by AFM. *Science* (in the press).
26. Kellermayer, M. S. Z., Smith, S. B., Granzier, H. L. & Bustamante, C. Folding-unfolding transitions in single titin molecules characterized with force-measuring laser tweezers. *Science* (in the press).

Acknowledgements. We thank M. Gautel, W. Gratzer, P. Knight, G. Offer, A. Pastore and D. Thomas for discussions and advice. Supported by BBSRC and NIH (J.T.), MRC (J.A.S. & R.M.S.) and the Human Frontier Science Program (R.M.S.).

Correspondence and requests for materials should be sent to R.M.S. (e-mail: r.simmons@kcl.ac.uk).

Crystal structure of ICAM-2 reveals a distinctive integrin recognition surface

José M. Casasnovas*, Timothy A. Springer*, Jin-huan Liu†‡, Stephen C. Harrison†§ & Jia-huai Wang†‡

** The Center for Blood Research, Harvard Medical School, Department of Pathology, 200 Longwood Avenue, Boston, Massachusetts 02115, USA*

† Department of Molecular and Cellular Biology, and § Howard Hughes Medical Institute, Harvard University, 7 Divinity Avenue, Cambridge, Massachusetts 02138, USA

Recognition by integrin proteins on the cell surface regulates the adhesive interactions between cells and their surroundings[1,2]. The structure of the 'I' domain that is found in some but not all integrins, has been determined[3,4]. However, the only integrin ligands for which structures are known, namely fibronectin and VCAM-1 (refs 5–7), are recognized by integrins that lack I domains. The intercellular adhesion molecules ICAM-1, 2 and 3 are, like VCAM-1, members of the immunoglobulin superfamily (IgSF), but they are recognized by an I domain-containing integrin, lymphocyte-function-associated antigen 1 (LFA-1, or CD11a/CD18). Here we present the crystal structure of the extracellular region of ICAM-2. The glutamic acid residue at position 37 is critical for LFA-1 binding and is proposed to coordinate the Mg^{2+} ion in the I domain; this Glu 37 is surrounded by a relatively flat recognition surface and lies in a β-strand, whereas the critical aspartic acid residue in VCAM-1 and fibronectin lie in protruding loops. This finding suggests that there are differences in the architecture of recognition sites between integrins that contain or lack I domains. A bend between domains 1 and 2 of ICAM-2 and a tripod-like arrangement of *N*-linked glycans in the membrane-proximal region of domain 2 may be important for presenting the recognition surface to LFA-1. A model of ICAM-1 based on the ICAM-2 structure provides a framework for understanding its recognition by pathogens.

The extracellular fragment of ICAM-2 containing the two predicted IgSF domains was expressed in lectin-resistant CHO Lec.3.2.8.1 cells[8] to obtain a homogeneous, high-mannose, *N*-linked glycoform. Crystallization trials were done with native and endoH-treated ICAM-2, and crystals were obtained only with the native protein. The structure was determined by multiple isomorphous replacement (MIR) and refined by XPLOR (see Methods and Table 1).

ICAM-2 has two domains with an immunoglobulin(Ig)-like fold (Fig. 1a). The molecule resembles a hockey stick, with a bend of 35° and a rotation of 152° between the N-terminal, membrane-distal domain 1 (D1), and the C-terminal, membrane-proximal domain 2 (D2), defined by superposition of the Ig framework. With domain 2 oriented perpendicular to the membrane, the edge of the two β-sheets formed by β-strands C and D in domain 1 faces outwards.

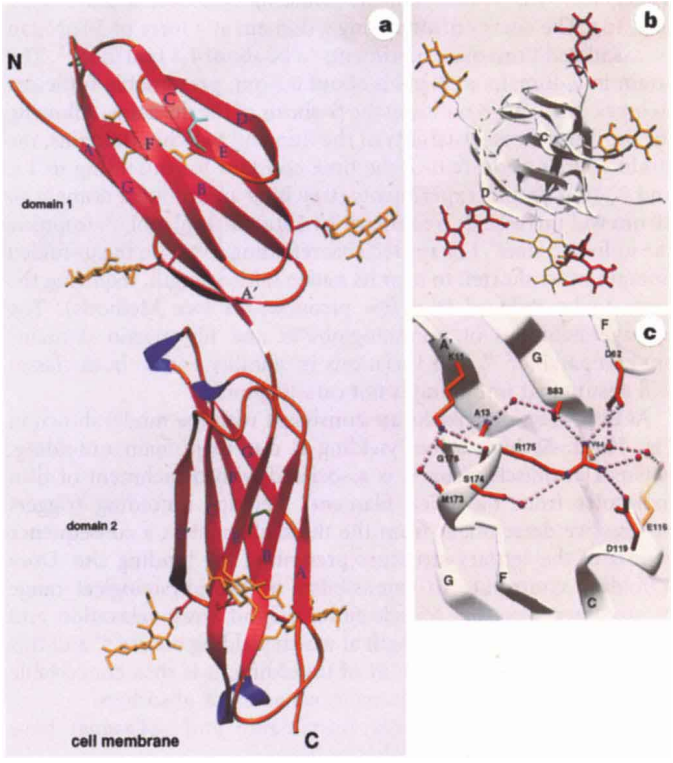

Figure 1 The crystal structure of ICAM-2. **a**, Ribbon diagram with β-strands in red, α-helix in blue and coil in orange. The last residue of domain 1 (Tyr 85) is white. *N*-linked sugars (yellow), Glu 37 in strand C of domain 1 (light blue) and disulphide bonds (green) are included. **b**, View from the top of domain 1 towards the membrane. Sugars linked to domains 1 and 2 are yellow and red, respectively. **c**, Hydrogen bonds between residues in domain 1 (top) and 2 (bottom). Nitrogen and oxygen atoms are in blue and red, respectively. Water molecules are shown as red spheres. Prepared with Ribbons[29].

‡ Present address: Dana-Farber Cancer Institute (J.-h.L. and J.-h.W.) and Children's Hospital (J.-h.W.), Harvard Medical School, 44 Binney Street, Boston, Massachusetts 02115, USA.

This edge bears Glu 37, which is the conserved acidic residue that is important for recognition of ICAMs by LFA-1 (refs 9–12).

ICAM-2 has a compact domain 1 and a relatively larger domain 2 (Fig. 1a). Domain 1 is composed of 85 residues and, like VCAM-1, falls into the I-set category of the IgSF[13]. Unlike typical I-set domains, ICAM2-D1 lacks a short C′ strand adjacent to strand C (Fig. 1a). Instead, the C strand turns directly into the CD loop and connects to the D strand across the β-barrel. This part of the molecule is therefore very flat. The four-residue deletion in the CD loop of ICAM2-D1 relative to VCAM-D1 (Fig. 2) presents a striking contrast in the display of the acidic residues that are critical for recognition by integrins. The acidic Glu 37 residue in ICAM-2 is the last residue in β-strand C, whereas the Asp 40 residue in VCAM-1 is at the upturned point of the CD loop (Fig. 2). The remarkably protruding CD loop on which Asp 40 is located in VCAM-1 has no equivalent in ICAM-2. These differences, and the alignment between all β-strands in VCAM-1 and ICAM-2 except for portions of two strands that differ in β-bulges, were correctly predicted on the basis of I-set framework residues (ref. 3, C. Chothia, personal communication). The conformation of the functionally important strands C, D and E in ICAM-2 differs from that in VCAM-1 (Fig. 2). In this part of the structure, the proportion of Cα carbons within 1.6 Å (asterisked in Fig. 2) is lower than for any other strand in the superimposed domains 1 or 2. There is an 'extra' disulphide bridge between Cys 28 (BC loop) and Cys 71 (end of the F strand) in ICAM-2 that creates a compact tip for domain 1. In VCAM-1, a similar disulphide-induced tapering has been proposed to make the ligand-binding region near the bottom of the domain more accessible[7].

Domain 2 of ICAM-2 belongs to the C2 set of IgSF domains, which is widely used by cell-surface molecules as building blocks to project the functional N-terminal domain away from the cell membrane[14]. As in VCAM-D2 (ref. 15), the conformation of the initial segment of domain 2 is fixed by two main-chain hydrogen bonds between Gln 86 and Glu 116 on the BC loop of domain 2. Glu 116 is followed by a *cis* proline that is conserved in ICAMs and VCAM-1 (Fig. 2). A particularly prominent FG loop in domain 2 of ICAM-2 cradles domain 1 (Fig. 1a). As in VCAM-D2 (refs 6, 7), the C′E and FG loops are unusually long for C2 set domains[14]. Except for the C′E and FG loops, ICAM2-D2 and VCAM1-D2 are remarkably similar, in contrast to D1 (Fig. 2).

Six *N*-linked high-mannose glycans, each predicted to contain about seven carbohydrate residues[8], are present per ICAM-2 molecule. The first two *N*-acetyl glucosamine residues are sufficiently ordered to be traced in the electron-density map and included in the structure (Fig. 1). ICAM-2 is among the most heavily glycosylated proteins in terms of sugar/protein ratio to be crystallized so far, with an average of one *N*-linked site per 32 amino-acid residues. Looking down the axis of the two IgSF domains, the six *N*-linked glycans are uniformly distributed around the perimeter of the domains (Fig. 1b). The three glycans in domain 1 are circumferential to the putative binding site around Glu 37 (Fig. 1a). The three glycosylation sites in domain 2 are quite evenly distributed (Fig. 1b, red) around its membrane proximal region (Fig. 1a). This 'tripod' arrangement and the large volume of the complete glycans will create a skirt around the base of D2, which is likely to orient ICAM-2 with respect to the cell surface so that domain 2 is perpendicular to the membrane and the integrin recognition surface in domain 1 is presented to interacting cells. A similar disposition of glycosylation sites is present in the second domain of mouse ICAM-2 (Fig. 2).

Crystallographic analysis of CD2 (ref. 16) and VCAM-1 (refs 6, 7) showed that the two independent copies of the molecules in the crystals differed in the orientation between domains 1 and 2 because of inherent interdomain flexibility. It is difficult to determine how flexible the interdomain linkage in ICAM-2 might be, because there is only one copy of the molecule in the asymmetric unit of the crystal. However, the hydrogen-bond network engaging the A′, G and F strands of domain 1 with residues in the FG and BC loops of domain 2 (Fig. 1c) is more extensive than in CD2 or VCAM-1 (refs 6, 7, 16). These interactions and the interdomain hydrophobic contacts involving Ala 13 and Tyr 85 from domain 1, and Leu 170, Leu 172 and Phe 180 from domain 2, may limit interdomain flexibility. In particular, multiple salt-bridges involving more than

Table 1 Crystallographic analysis

	Native	Derivatives		
		C_2H_5HgCl (0.5 mM)	$K_2Pt(C_2O_4)_2$ (1 mM)	$(CH_3)_3PbAc$ (25 mM)
Resolution (Å)	15–2.2	15–2.5	15–3.5	15–3.5
Completeness (%)	93.9 (68.8)	90.0	98.0	95.0
Redundancy	3.1	3.0	3.8	2.8
R_{merge}*	0.044 (0.141)	0.055	0.103	0.069
R_{der}†		0.129	0.207	0.208
PP‡		0.70	0.80	1.0
R_c§		0.85	0.89	0.70
Refinementǁ				
Model	192 amino-acid residues, 12 NAG and 142 water molecules			
Resolution range (Å)	15.0–2.2			
R factor (%)	22.6 (29.5 free *R*)			

Completeness and *R* merge for the outermost shell (2.32–2.2 Å) of the native data are in parentheses.
* $R_{merge} = \Sigma_{hkl}\Sigma i|Ii_{hkl} - I_{hkl}|/\Sigma hkl Ii_{hkl}$.
† $R_{der} = \Sigma i|F_{PH} - F_P|/\Sigma i F_P$, where F_P and F_{PH} refer to the measured structure amplitudes of the native and derivatives.
‡ PP: phasing power, mean value of the heavy-atom structure amplitudes divided by the residual lack-of-closure.
§ R_c: Cullis *R* factor for centric reflections; $R_c = \Sigma[|F_H| - (|F_{PH} - F_P|)]/\Sigma|F_H|$. Figure of merit was 0.37 for acentric reflections and 0.66 for centric ones.
ǁ Reflections with $F > 2\sigma$ were used in refinement. 10% of reflections were selected for determination of free *R* factor.

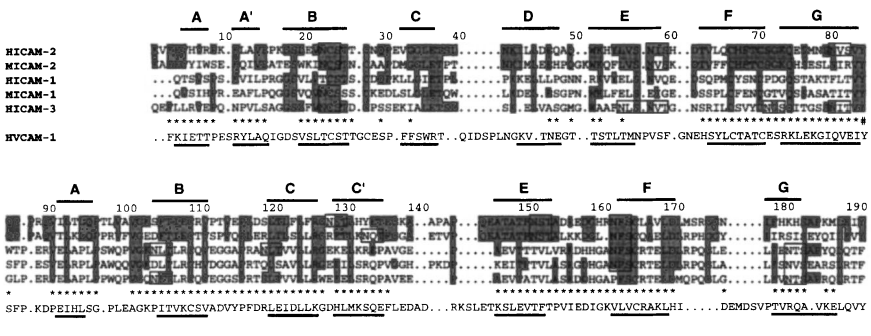

Figure 2 The secondary structure of ICAM-2 and alignment with ICAMs and VCAM-1. β-strands defined by the program DSSP for ICAM-2 and VCAM-1 (ref. 7) are represented by lines. Residues of ICAM-2 conserved in other aligned ICAMs are shaded. Putative *N*-linked glycosylation sites are framed. ICAM-2 and VCAM-1 were structurally superimposed using the 3DMALIGN module of MODELLER[31], independently for domain 1 (top) and domain 2 (bottom). In the structure-based alignment with VCAM-1, only residues with Cα carbons within 4 Å of one another are aligned, and those within 1.6 Å are marked with asterisks. The conserved Tyr 85 (indicated by a hash sign) was close (~1 Å) to its counterpart in VCAM-1 when structural superposition was based on D2.

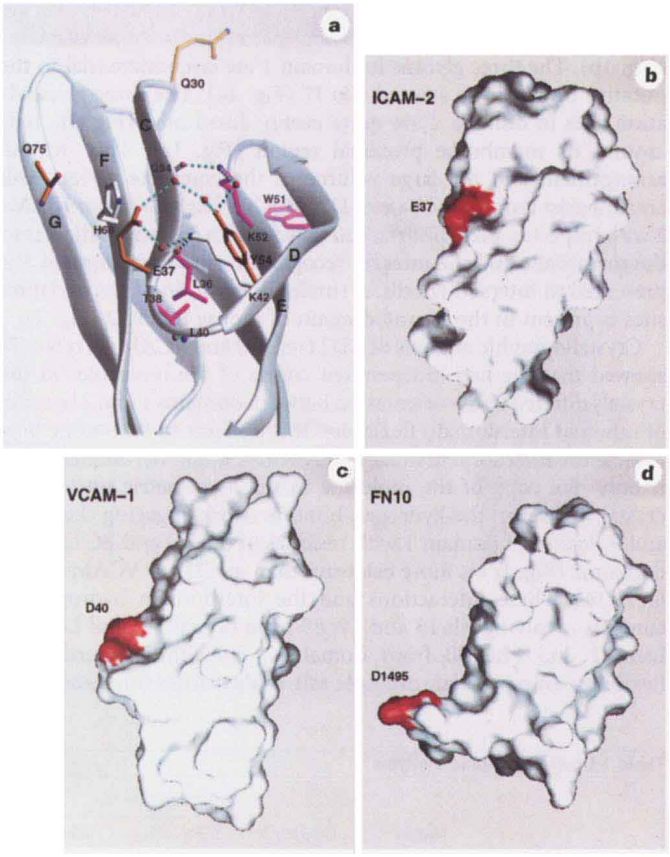

Figure 3 The integrin-binding surface in ICAM-2 and molecular surface representations of integrin ligands. **a**, Residues involved in binding to LFA-1 (orange), domain conformation (magenta) and close to Glu 37 (white) are included. Hydrogen bonds between residues or water molecules (red spheres) are presented as shaded light blue cylinders. Atoms are as in Fig. 1c. Prepared with Ribbons[29]. **b**–**d**, Molecular surface representations of integrin-binding domains for ICAM-2, VCAM-1 and fibronectin domain 10 are shown with the acidic residue involved in binding coloured in red. Molecular surfaces were created with GRASP[30]. Note that the protruding integrin-binding region in VCAM-1 is in the CD loop, whereas in fibronectin it is in the FG loop.

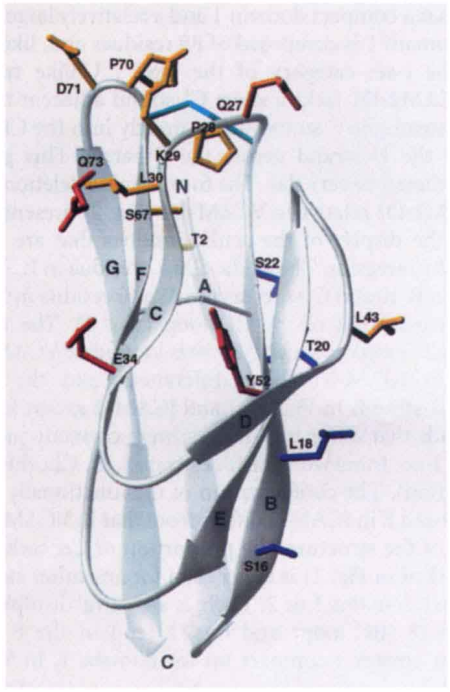

Figure 4 Ligand recognition by ICAM-1. A model of the N-terminal domain of ICAM-1 was constructed with a segment modelling program (Look, Molecular Applications Group) based on the alignment with ICAM-2 shown in Fig. 2. Residues involved in rhinovirus, LFA-1 and PFIE binding are coloured in yellow, red and blue, respectively. Q27, a residue important for LFA-1 and HRV binding, is in orange. Single amino-acid mutations, except the double mutation T20 and S22, with a significant influence in binding (>40% decrease binding compared with wild type) have been included. The 'extra' disulphide bond in the domain is in cyan.

two charged residues[17] centred at Arg 175 (Fig. 1c) are found at the domain interface. The interdomain interactions create a bent conformation for the two-domain module in the crystal structure, with the CD edge of domain 1 and Glu 37 projecting toward the top, optimally presented for adhesive interactions (Fig. 1a). The 35° bend in ICAM-2 compares to bends of 13 to 41° for CD2 (ref. 16) and 5° to 35° for VCAM-1 (refs 6, 7). Also, the rotation between domain 1 and 2 differs, making the C′E loop in domain 2 of ICAM-2 more distant from the CD edge of domain 1 than in VCAM-1.

The strong sequence conservation around Glu 37 in other ICAMs (Fig. 2) suggests that the conformation of their integrin-binding surfaces will be similar to that of ICAM-2. The hydrogen bond between the hydroxyl group of the highly conserved Thr 38 (Fig. 2) and the main chain -NH of Leu 40 positions Glu 37 and helps to determine the CD loop conformation (Fig. 3a). Mutagenesis studies of ICAMs[9–12] have shown that four conserved residues are important for adhesive interactions with LFA-1 (orange in Fig. 3a). Glu 37, the most critical residue for integrin binding, is the last residue of the C strand in domain 1 of ICAM-2. Tyr 54 on the E strand and Gln 30 in the BC loop are located at the exposed CD edge of the β-barrel. Gln 75 is on the G strand, with its side chain facing Glu 37. These residues define a broad area that includes the CD edge and the GFC-β-sheet of the domain. Structural and functional data show that residues in the I domain of LFA-1 involved in binding to ICAM-1 lie on both sides of the bound Mg^{2+} (refs 3, 4, 18). Therefore, the disposition of the binding residues in ICAMs and the I domain of LFA-1 are consistent with the notion that Glu 37 in ICAM-2 and the Mg^{2+} in the I domain could coordinate in the centre of the binding interface.

The flat surface of ICAM-2 surrounding Glu 37 (Fig. 3b) complements well in shape the relatively flat surface surrounding the Mg^{2+} in the I domains of Mac-1 and LFA-1 (refs 3, 4). By contrast, in the non-I-domain integrin ligands VCAM-1 (Fig. 3c) and fibronectin (Fig. 3d), the Asp residues involved in binding are located in protruding loops[5–7]. These differences in presentation of integrin-binding motifs by integrin ligands may therefore reflect general differences in the ligand-binding site between I-domain- and non-I-domain-containing integrins. This difference correlates with the prediction that non-I-domain integrin ligands bind to a β-propeller domain in integrin α-subunits, which contains a putative binding pocket[19].

In addition to serving as a ligand for LFA-1, ICAM-1 is the cell-surface receptor for the major group of human rhinovirus (HRV)[20,21] and a receptor for sequestration of *Plasmodium falciparum*-infected

erythrocytes in the peripheral vasculature[22]. Residues involved in the recognition of all these three ligands lie mainly in the N-terminal domain of the receptor[9,23–26]. A model of ICAM-1 based on domain 1 of ICAM-2 suggests that the rhinovirus[9,23,24] and LFA-1 (refs 9, 11) binding surfaces are distinct but overlapping (yellow and red, respectively, in Fig. 4), as previously predicted from mutagenesis data. By contrast, residues involved in binding to *P. falciparum*-infected erythrocytes (blue)[25,26] are in the B strand, on the edge of the domain opposite the LFA-1 binding surface. *Plasmodium*-derived proteins seem to recognize a linear and narrow epitope surface, consistent with the ability of peptides like G15SVLV to block ICAM-1 binding[25]. Lack of glycosylation in domain 1 of human ICAM-1 compared to ICAM-2 and ICAM-3 may be an important determinant of the promiscuity of this cell-adhesion molecule in terms of recognition by microorganisms. The crystal structure of ICAM-2 may therefore advance the development of therapeutics for treatment of immunological and vascular disorders and pathogenic infections. □

Methods

Protein expression, purification and crystallization. A recombinant ICAM-2 cDNA with a translation stop codon in the position of Glu 196 was generated by PCR from the plasmid pCDIC2.27 (ref. 27), and introduced into the unique *Xho*I–*Not*I site of pBJ5-GS[28], to obtain pBJ5-GS/ICAM-2. A CHO cell mutant (CHO Lec3.2.8.1) with highly restricted glycosylation was transfected with pBJ5-GS/ICAM-2 using calcium phosphate, and clones secreting soluble ICAM-2 were selected[28]. ICAM-2 was purified from the cell supernatant by immunoaffinity with CBR-IC2/2 mAb and size-exclusion chromatography, essentially as described for ICAM-1 (ref. 28). Two major species of 37.5K and 35.9K were seen in SDS–PAGE and were cleaved to 27.8K and 26.4K with endoglycosidase H and N-glycanase, respectively. The N-terminal sequence of ICAM-2, which had not been previously determined, is KVFEV. Therefore, the signal sequence is three residues longer than previously predicted from the cDNA sequence[27] and the recombinant soluble ICAM-2 contains 192 amino acid residues (Fig. 2).

Crystals were grown best at 4 °C using the hanging-drop vapour diffusion method, with a protein solution of 15–17 mg ml^{-1} and a crystalization solution with 20% PEG 4000, 20 mM cacodylate buffer, pH 6.4, and 25 mM β-octyl-glucopyranoside. They belong to space group *C*2 ($a = 69.0$ Å, $b = 63.7$ Å, $c = 76.2$ Å and $\beta = 114.5°$), with one molecule per asymmetric unit and 45% solvent by volume. Crystals were frozen under − 160 °C liquid nitrogen cold stream for data collection using 20% ethylene glycol as cryoprotectant.

Structure determination and refinement. Each data set was collected from a single frozen crystal, using a Siemens/Nicolet area detector equipped with an Elliott GX-13 rotating anode X-ray generator. Raw data were reduced using XDS and further processed with CCP4 suite (SERC collaborative computer project 4; Daresbury Laboratory, Daresbury, UK).

The structure was determined by the MIR method using three heavy-atom derivatives: ethyl mercury chloride, trimethyl lead acetate and potassium bis(oxalato)-platinate. Heavy-atom parameters were determined by difference Patterson and difference Fourier and refined with HEAVY and MLPHARE. Phase statistics are listed in Table 1. The initial MIR map at 3.5 Å was of poor quality, although protein–solvent boundaries were detected. This map was dramatically improved by applying a density modification procedure as implemented in the CCP4 program DM (SERC CCP4). After the first model was built, a second run of DM with a more accurate envelope further improved the map on which a complete ICAM-2 molecule was built, except for the C′E-loop of D2.

X-PLOR (a system for crystallography and NMR, New Haven, CT, version 3.1) was used to carry out the structure refinement, alternated by manual model rebuilding. A resolution range from 15 to 3 Å was first used and was extended stepwise to 2.2 Å. Both energy minimization and simulated annealing options were applied and at a very late stage only energy minimization was done. Solvent mask correction was made during refinement. An overall anisotropic temperature factor was applied to F_o to obtain the best results.

The current model contains all 192 amino-acid residues, 12 *N*-acetyl glucosamines (NAG) residues and 142 water molecules with good geometry (r.m.s. deviations for bond length and bond angles are 0.019 Å and 2.2°, respectively). Only two residues (Ala 140 and Gln 145) that lie on the poorly defined C′E loop have disallowed main-chain torsion angles in the Ramachandran plot of our model. Quite good density is present for the first NAG at high contour (1.2σ) and for the second one at low contour (>0.7σ). The missing sugar residues in our model account for 20% of the molecular weight of the protein and may contribute to the *R* factor of our model, particularly at the low-resolution bin.

Received 7 January; accepted 17 March 1997.

1. Hynes, R. O. Integrins: Versatility, modulation, and signaling in cell adhesion. *Cell* **69,** 11–25 (1992).
2. Springer, T. A. Traffic signals for lymphocyte recirculation and leukocyte emigration: The multi-step paradigm. *Cell* **76,** 301–314 (1994).
3. Lee, J.-O., Rieu, P., Arnaout, M. A. & Liddington, R. Crystal structure of the A domain from the α-subunit of integrin CR3 (CD11b/CD18). *Cell* **80,** 631–638 (1995).
4. Qu, A. & Leahy, D. J. Crystal structure of the I-domain from the CD11a/CD18 (LFA-1, $a_l b2$) integrin. *Proc. Natl Acad. Sci. USA* **92,** 10277–10281 (1995).
5. Leahy, D. J., Aukhil, I. & Erickson, H. P. 2.0 Å crystal structure of a four-domain segment of human fibronectin encompassing the RGD loop and synergy region. *Cell* **84,** 155–164 (1996).
6. Jones, E. Y. *et al.* Crystal structure of an integrin-binding fragment of vascular cell adhesion molecule-1 at 1.8 Å resolution. *Nature* **373,** 539–544 (1995).
7. Wang, J.-h. *et al.* The crystal structure of an N-terminal two domain fragment of VCAM-1: A cyclic peptide based on the domain 1 C-D loop can inhibit VCAM-1/α4 integrin. *Proc. Natl Acad. Sci. USA* **92,** 5714–5718 (1995).
8. Stanley, P. Chinese hamster ovary cell mutants with multiple glycosylation defects for production of glycopoteins with minimal carbohydrate heterogeneity. *Mol. Cell. Biol.* **9,** 377–383 (1989).
9. Staunton, D. E., Dustin, M. L., Erickson, H. P. & Springer, T. A. The arrangement of the immunoglobulin-like domains of ICAM-1 and the binding sites for LFA-1 and rhinovirus. *Cell* **61,** 243–254 (1990).
10. Holness, C. L. *et al.* Analysis of the binding site on intercellular adhesion molecule 3 for the leukocyte integrin lymphocyte function-associated antigen 1. *J. Biol. Chem.* **270,** 877–884 (1995).
11. Klickstein, L. B., York, M. B., de Fougerolles, A. R. & Springer, T. A. Localization of the binding site on intercellular adhesion molecule-3 (ICAM-3) for lymphocyte function-associated antigen-1 (LFA-1). *J. Biol. Chem.* **271,** 23920–23927 (1996).
12. Sadhu, Ç. *et al.* LFA-1 binding site in ICAM-3 contains a conserved motif and non-contiguous amino acids. *Cell Adhes. Commun.* **2,** 429–440 (1994).
13. Harpaz, Y. & Chothia, C. Many of the immunoglobulin superfamily domains in cell adhesion molecules and surface receptors belong to a new structural set which is close to that containing variable domains. *J. Mol. Biol.* **238,** 528–539 (1994).
14. Williams, A. F. A year in the life of the immunoglobulin superfamily. *Immunol. Today* **8,** 298–303 (1987).
15. Wang, J.-h. *et al.* Structure of a functional fragment of VCAM-1 refined at 1.9 Å resolution. *Acta Crystallogr.* **52,** 369–379 (1996).
16. Bodian, D. L., Jones, E. Y., Harlos, K., Stuart, D. I. & Davis, S. J. Crystal structure of the extracellular region of the human cell adhesion molecule CD2 at 2.5 Å resolution. *Structure* **2,** 755–766 (1995).
17. Musafia, B., Buchner, V. & Arad, D. Complex salt bridges in proteins: Statistical analysis of structure and function. *J. Mol. Biol.* **254,** 761–770 (1995).
18. Huang, C. & Springer, T. A. A binding interface on the I domain of lymphocyte function associated antigen-1 (LFA-1) required for specific interaction with intercellular adhesion molecule 1 (ICAM-1). *J. Biol. Chem.* **270,** 19008–19016 (1995).
19. Springer, T. A. Folding of the N-terminal, ligand-binding region of integrin α-subunits into a β-propeller domain. *Proc. Natl Acad. Sci. USA* **94,** 65–72 (1997).
20. Greve, J. M. *et al.* The major human rhinovirus receptor is ICAM-1. *Cell* **56,** 839–847 (1989).
21. Staunton, D. E. *et al.* A cell adhesion molecule, ICAM-1, is the major surface receptor for rhinoviruses. *Cell* **56,** 849–853 (1989).
22. Berendt, A. R., Simmons, D. L., Tansey, J., Newbold, C. I. & Marsh, K. Intercellular adhesion molecule-1 is an endothelial cell adhesion receptor for Plasmodium falciparum. *Nature* **341,** 57–59 (1989).
23. McClelland, A. *et al.* Identification of monoclonal antibody epitopes and critical residues for rhinovirus binding in domain 1 of intercellular adhesion molecule 1. *Proc. Natl Acad. Sci. USA* **88,** 7993–7997 (1991).
24. Register, R. B., Uncapher, C. R., Naylor, A. M., Lineberger, D. W. & Colonno, R. J. Human-murine chimeras of ICAM-1 identify amino acid residues critical for rhinovirus and antibody binding. *J. Virol.* **65,** 6589–6596 (1991).
25. Ockenhouse, C. F., Betageri, R., Springer, T. A. & Staunton, D. E. *Plasmodium falciparum*-infected erythrocytes bind ICAM-1 at a site distinct from LFA-1, Mac-1, and human rhinovirus. *Cell* **68,** 63–69 (1992).
26. Berendt, A. R. *et al.* The binding site on ICAM-1 for plasmodium falciparum-infected erythorcytes overlaps, but is distinct from, the LFA-1-binding site. *Cell* **68,** 71–81 (1992).
27. Staunton, D. E., Dustin, M. L. & Springer, T. A. Functional cloning of ICAM-2, a cell adhesion ligand for LFA-1 homologous to ICAM-1. *Nature* **339,** 61–64 (1989).
28. Casasnovas, J. M. & Springer, T. A. Kinetics and thermodynamics of virus binding to receptor: Studies with rhinovirus, intercellular adhesion molecule-1 (ICAM-1), and surface plasmon resonance. *J. Biol. Chem.* **270,** 13216–13224 (1995).
29. Carson, M. Ribbon models of macromolecules. *J. Mol. Graph.* **5,** 103–106 (1987).
30. Nicholls, A., Sharp, K. A. & Honig, B. Protein folding and association; insights from the interfacial and thermodynamic properties of hydrocarbons. *Proteins* **11,** 281–296 (1991).
31. Sali, A. Thesis, Univ. London, 1991.

Acknowledgements. We thank S. Martin and D. Staunton for recombinant cDNA, J. Bickford for technical assitance; P. Stanley for mutant CHO cells; and the members of S.C.H.'s group for helpful discussions, especially T. Stehle, D. Rodgers and B. Harris. This work was supported by grants from the NIH. S.C.H. is an investigator of the Howard Hughes Medical Institute.

Correspondence should be addressed to J.H.W. and requests for materials should be addressed to T.A.S. The ID code for the ICAM-2 coordinates in the Protein Data Bank is 1ZXQ.